ISSN 1063-7834, Physics of the Solid State, 2007, Vol. 49, No. 1, pp. 34–38. © Pleiades Publishing, Ltd., 2007.
Original Russian Text © A.V. Malakhovskiĭ, A.É. Sokolov, A.L. Sukhachev, V.L. Temerov, N.A. Stolbovaya, I.S. Edelman, 2007, published in Fizika Tverdogo Tela, 2007, Vol. 49, No. 1, pp. 32–36.

SEMICONDUCTORS AND DIELECTRICS

Magnetic Circular Dichroism and Optical Absorption in $TmAl_3(BO_3)_4$

A. V. Malakhovskiĭ, A. É. Sokolov, A. L. Sukhachev, V. L. Temerov, N. A. Stolbovaya, and I. S. Edelman

Kirensky Institute of Physics, Siberian Division, Russian Academy of Sciences, Krasnoyarsk, 660036 Russia
e-mail: ise@iph.krasn.ru

Received February 7, 2006

Abstract—The polarized spectra of absorption and magnetic circular dichroism in a $TmAl_3(BO_3)_4$ single crystal are studied in the region of $^3H_6 \longrightarrow {}^3F_4$, $^3H_6 \longrightarrow {}^3F_3$, and $^3H_6 \longrightarrow {}^3F_2$ electronic transitions in the Tm^{3+} ion. The structure of the spectra is interpreted qualitatively. It is shown that the magnetic circular dichroism of the $^3H_6 \longrightarrow {}^3F_4$ transition is determined by the contribution from the splitting of the ground state, whereas the magnetic circular dichroism of the $^3H_6 \longrightarrow {}^3F_3$ transition is governed by the contribution from the splitting of an excited state in a trigonal crystal field.

PACS numbers: 78.20.-e, 78.40.Ha, 75.50.Ee

DOI: 10.1134/S1063783407010076

1. INTRODUCTION

Crystals doped by rare-earth ions or containing rare-earth ions in the stoichiometric composition have been attracting considerable interest due to their vast application potential, including as laser media. The basic processes responsible for emission in the spectral regions of interest are currently known. However, the spectroscopic properties of rare-earth ions in the crystal matrix and their luminescence characteristics depend strongly on the structure of the matrix, i.e., on the environment of the rare-earth ions and their concentration in the crystal. This is why the desired set of optical properties of a material still cannot be predicted with reasonable accuracy, which makes it necessary to conduct an experimental study of the newly synthesized compound in each particular case. In recent years, there has been an explosive interest in aluminoborates of the general formula $RAl_3(BO_3)_4$ (with a structure of the huntite mineral $CaMg_3(CO_3)_4$ [1]), where R stands for a rare-earth element. The crystals have trigonal symmetry with space group $R32$ (No. 155 of the International Tables for X-Ray Crystallography). The unit cell contains three formula units ($Z = 3$). Trivalent rare-earth ions occupy only one type of position of symmetry D_3. These ions are located at the center of a trigonal prism made up of six crystallographically equivalent oxygen ions. Each oxygen ion in the environment of the rare-earth ion belongs to its own borate group. The triangles formed by the oxygen ions in the base and top planes are not superimposed but twisted by some distortion angle. Owing to this distortion, the D_{3h} symmetry of the ideal prism is reduced to D_3.

The majority of studies performed in this field have dealt with crystals doped by Nd, Gd, Tb, and Yb, as well as with those containing these elements in the stoichiometric composition [2–6]. At the same time, it is known that, in other compounds, Tm^{3+} is characterized by radiative transitions in various (from ultraviolet to infrared) spectral regions [7–15]. This has stirred considerable interest in the optical spectra of $TmAl_3(BO_3)_4$. As regards the magneto-optical properties of Tm^{3+} ions, they have not been studied thus far at all, even though understanding the nature of the magneto-optical activity of electronic transitions in rare-earth ions is an issue of fundamental importance.

The purpose of this work was to investigate the absorption spectra and magnetic circular dichroism of Tm^{3+} in a synthesized single crystal of $TmAl_3(BO_3)_4$ and to interpret the spectra obtained.

2. SAMPLE PREPARATION

Single crystals of $TmAl_3(BO_3)_4$ were grown from a melt solution based on bismuth trimolybdate and lithium molybdate used previously to prepare $(Tb,Er)_xFe_{3-x}Ga_5O_{12}$ garnets doped with rare-earth ions [16]:

$$\{85\ \text{wt}\ \%\ [Bi_2Mo_3O_{12} + 2B_2O_3 + 0.5Li_2MoO_4] + 15\ \text{wt}\ \%\ TmAl_3(BO_3)_4\}.$$

The saturation temperature of the melt solution was $T_{sat} \approx 1000$°C. The concentration dependence of the saturation temperature had a slope $dT_{sat}/dn \approx 15$°C/wt %. The metastable zone was about 20°C wide. The melt solution (total weight, 1 kg) was prepared in a cylindrical platinum crucible ($D = 100$ mm, $H = 90$ mm). The

melting and homogenization stages were limited by the temperatures $T = 1050$–1100°C. The saturation temperature was determined accurate to within ±2°C with the use of trial crystals grown previously through spontaneous nucleation.

Several crystals were grown at a time. Eleven seeds ≈1 mm^3 in volume were fixed to a ring crystal holder. The initial supercooling was 10°C, which corresponded to the center of the metastability zone. After this, the temperature of the melt solution was decreased at an increasing rate of 1–3°C/day. The crystal growth rate did not exceed 0.5 mm/day. The crystal holder was rotated reversibly with a 1-min period. After the growth was complete, the crystal holder was raised above the melt solution and the furnace was left to cool to room temperature with the power supply turned off. Crystals measuring 6–10 mm with a total mass of 15 g were obtained in the crystallization temperature range of 17°C. The lattice constants of the crystals synthesized were determined from x-ray diffraction measurements: $a = 9.280(1)$ Å and $c = 7.211(1)$ Å.

The samples prepared for measurements were ≈0.15-mm-thick plane-parallel polished platelets oriented perpendicular or parallel to the threefold crystallographic axis.

3. EXPERIMENTAL RESULTS AND DISCUSSION

The absorption spectra were measured at room temperature in the frequency range 12000–16000 cm^{-1} with light propagating along the C_3 axis (the α spectrum) and normal to the plane aligned with the C_3 axis for the light wave vector $\mathbf{E}$ parallel (the π spectrum) and perpendicular (the σ spectrum) to the C_3 axis of the crystal. The spectral resolution was ~10 cm^{-1}. An Ahrens prism served as a polarizer. The magnetic circular dichroism spectrum was recorded with light propagating along the C_3 axis of the crystal. The magnetic field was 2.5 kOe. The magnetic circular dichroism was measured by modulating the light polarization with a piezomodulator. The accuracy in measuring the magnetic circular dichroism was 10^{-4}, and the spectral resolution was ~50 cm^{-1}.

The absorption spectra obtained in the π and σ polarizations are shown in Fig. 1 for the $^3H_6 \longrightarrow {}^3F_4$ transition and in Fig. 2 for the $^3H_6 \longrightarrow {}^3F_3$ and $^3H_6 \longrightarrow {}^3F_2$ transitions. The absorption spectra measured in the polarizations σ and α coincide. This implies that the absorption occurs through the electric dipole mechanism. The absorption spectra are decomposed into Gaussian components. The parameters of the strongest absorption lines are listed in the table. The designations of the splitting components A_1–A_{10}, B_1–B_9, and C_1–C_3 for the first, second, and third of the above bands were introduced for convenience in the subsequent discussion. We readily see substantial differences in the integrated band intensity and intensity distribution among the components in the π and σ spectra, as well as a dif-

Parameters of the absorption bands in the spectrum of $TmAl_3(BO_3)_4$

Transition	Notation	Energy, cm^{-1}	Polarization	Width, cm^{-1}	Integrated intensity, cm^{-2}
$^3H_6$–$^3F_4$	A	–	σ	–	6110
		–	π	–	3130
	A_3	12320	σ	59	650
		12319	π	50	100
	A_4	12373	σ	41	930
		12375	π	45	360
	A_5	12422	σ	31	160
		12430	π	35	45
	A_6	12465	σ	83	1620
		12477	π	87	980
	A_7	12545	σ	25	330
		12545	π	25	310
	A_8	12640	σ	125	1070
		12626	π	88	990
	A_9	12740	σ	40	190
		12731	π	44	130
	A_{10}	12811	σ	60	690
		12799	π	61	170
$^3H_6$–$^3F_3$	B	–	σ	–	7300
		–	π	–	4900
	B_1	14015	σ	82	280
		14302	π	86	170
	B_3	14179	σ	26	190
		14172	π	21	40
	B_4	14219	σ	33	320
		14215	π	70	260
	B_5	14315	σ	69	1340
		14321	π	39	1000
	B_6	14402	σ	47	1030
		14403	π	53	630
	B_7	14449	σ	32	970
		14449	π	38	700
	B_8	14500	σ	38	1550
		14506	π	44	1130
	B_9	14576	σ	93	540
		14583	π	90	410
$^3H_6$–$^3F_2$	C	–	σ	–	510
		–	π	–	350
	C_1	14948	σ	50	240
		14941	π	66	130
	C_2	15029	σ	49	150
		15038	π	56	110
	C_3	15121	σ	45	120
		15119	π	31	110

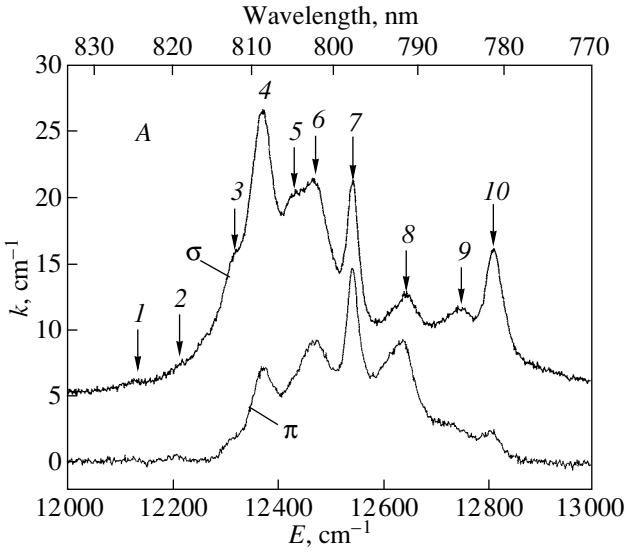

Fig. 1. Absorption spectra measured in the π and σ polarizations for the ${}^3H_6 \longrightarrow {}^3F_4$ transition (*A* band).

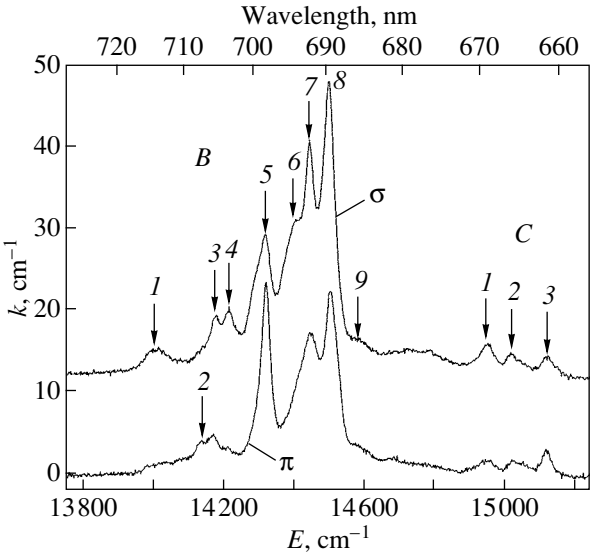

Fig. 2. Absorption spectra measured in the π and σ polarizations for the ${}^3H_6 \longrightarrow {}^3F_3$ (*B* band) and ${}^3H_6 \longrightarrow {}^3F_2$ (*C* band) transitions.

ference between the π and σ spectra themselves, i.e., dichroism (Figs. 1, 2). Some lines are revealed either only in the π polarization or only in the σ polarization. All the above transitions are forbidden for a free ion in the electric dipole approximation both in the parity and in the total momentum in accordance with the selection rule $\Delta J = 0 \pm 1$, with this forbiddenness being the stronger, the smaller the total momentum of the excited state. The integrated intensity of the transitions decreases in about the same order (see table). According to the Judd–Ofelt theory, the odd component of the crystal field lifts the parity forbiddenness from transitions with $\Delta J \le \lambda$, where $\lambda = 2, 4, 6$ for *f–f* transitions.

As was mentioned in Section 1, thulium ions, like the other rare-earth ions in the huntite structure, are contained inside a trigonally distorted noncentrosymmetric oxygen octahedron [4]. Therefore, in order to interpret the spectra obtained, we consider the splitting of states (and the corresponding absorption lines) in two steps: first, the splitting of states in the crystal field of the *O* symmetry, and, then, further splitting of states in the D_3 crystal field, which describes the local symmetry of the environment of the thulium ion. One should consider the noncentrosymmetric octahedral *O* crystal field rather than the O_h crystal field, because, in this case, *f–f* transitions would already be parity-allowed. It is primarily static distortions rather than vibrations that usually lift forbiddenness from the *f–f* transitions [17]. Below, we present the splitting schemes for the ground state and the three excited states studied [18].

For ${}^3H_6$ with the *O* field,

$$\Gamma_1 + \Gamma_2 + \Gamma_3 + \Gamma_4 + 2\Gamma_5, \qquad (1)$$

and the D_3 field,

$$\Gamma_1 + \Gamma_2 + \Gamma_3 + (\Gamma_2 + \Gamma_3) + 2(\Gamma_1 + \Gamma_3). \qquad (2)$$

For ${}^3F_4$ with the *O* field,

$$\Gamma_1 + \Gamma_3 + \Gamma_4 + \Gamma_5, \qquad (3)$$

and with the D_3 field,

$$\Gamma_1 + \Gamma_3 + (\Gamma_2 + \Gamma_3) + (\Gamma_1 + \Gamma_3). \qquad (4)$$

For ${}^3F_3$ with the *O* field,

$$\Gamma_2 + \Gamma_4 + \Gamma_5, \qquad (5)$$

and with the D_3 field,

$$\Gamma_2 + (\Gamma_2 + \Gamma_3) + (\Gamma_1 + \Gamma_3). \qquad (6)$$

For ${}^3F_2$ with the *O* field,

$$\Gamma_3 + \Gamma_5, \qquad (7)$$

and with the D_3 field,

$$\Gamma_3 + (\Gamma_1 + \Gamma_3). \qquad (8)$$

In order for a transition to be allowed, the representation of the transition operator

$$\Gamma_t = \Gamma_i \Gamma_f, \qquad (9)$$

where Γ_i and Γ_f are the representations of the initial and final states, respectively, should contain either the representation of the electric dipole moment Γ_4 (in the octahedral group) or the representation of the electric dipole moment components Γ_2 for the π polarization and Γ_3 for the σ polarization (in the D_3 group). According to representation (9), the allowed transitions in the

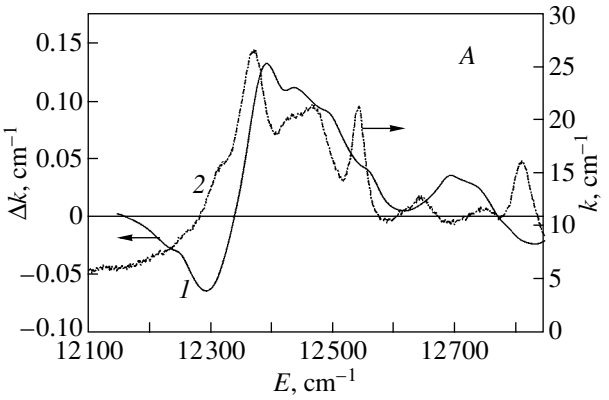

Fig. 3. (*1*) Magnetic circular dichroism and (*2*) absorption spectra measured in the α polarization for the $^3H_6 \longrightarrow {}^3F_4$ transition (*A* band).

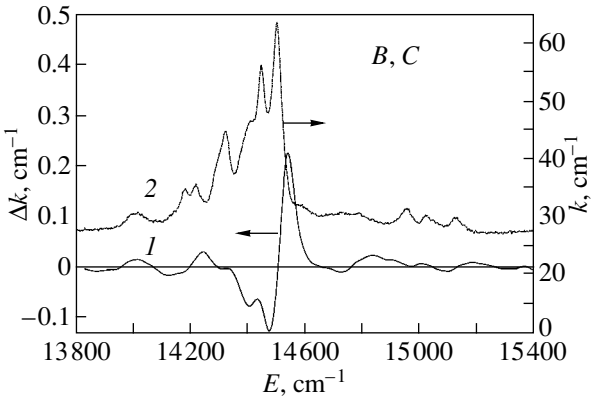

Fig. 4. (*1*) Magnetic circular dichroism and (*2*) absorption spectra measured in the α polarization for the $^3H_6 \longrightarrow {}^3F_3$ (band *B*) and $^3H_6 \longrightarrow {}^3F_2$ (band *C*) transitions.

octahedral symmetry are $\Gamma_4, \Gamma_5 \longrightarrow \Gamma_4, \Gamma_5$; $\Gamma_1 \longleftrightarrow \Gamma_4$, $\Gamma_2 \longleftrightarrow \Gamma_5$, and $\Gamma_3 \longleftrightarrow \Gamma_4, \Gamma_5$. Note that these transitions, of course, can occur in both polarizations. Hence, it follows from schemes (1), (3), (5), and (7) that the $^3H_6 \longrightarrow {}^3F_4$ and $^3H_6 \longrightarrow {}^3F_3$ transitions are responsible for 14 and 12 lines of this kind, respectively, whereas the $^3H_6 \longrightarrow {}^3F_2$ transition gives rise to 8 lines. Furthermore, as is evident from schemes (2), (4), (6), and (8) and transition operator (9), a lowering of the symmetry to trigonal can bring about an additional splitting of these lines, as well as allow transitions that are forbidden in the octahedral crystal field. Since the trigonal crystal field is only a small distortion of the octahedron, these additional transitions should be weak and may not be observable at all. Indeed, the observed number of lines (Figs. 1, 2) is even smaller than that conditioned by the octahedral crystal field. Nonetheless, lowering the symmetry brings about a noticeable dichroism. At first glance, this situation might seem strange. However, the low-symmetry component, which plays the role of only a small addition to the cubic crystal field in the distribution of the level splitting, is the sole source of intensity of the *f*–*f* transitions. The separations between the extreme lines in bands *A*, *B*, and *C* (~690, 580, and 170 cm^{-1} or 993, 835, and 250 K, respectively) make minimum contributions to the total crystal-field splittings of the ground and excited states.

The magnetic circular dichroism spectra of the transitions responsible for bands *A* and *B* (see Figs. 3 and 4, respectively) differ radically. The integrated magneto-optical activity is defined as the ratio of the integrated magnetic circular dichroism to the integrated absorption of bands *A* and *B* in the α (σ) polarization. Measured in units of $\mu_B H/kT$, the integrated magneto-optical activity is 4.9 and 1.8, respectively. Thus, the integrated magneto-optical activity for the transition in band *B* is close to one-third of that of the transition in band *A*.

In the general case, the magnetic circular dichroism is a sum of three terms:

$$\Delta D = A(\lambda) + B(\lambda) + C(\lambda, T). \quad (10)$$

The diamagnetic term *A* is proportional to the splitting of electronic states in the magnetic field and is independent of temperature. The paramagnetic term *C* is proportional to the difference between the thermal populations of the splitting components of the ground state in the magnetic field and, therefore, is a function of temperature. Since the term *B* originates from the polarization of the transitions in the magnetic field, it has the same dispersion as the term *C* and is also called paramagnetic. This term appears as a result of a mixing of states by the magnetic field and, therefore, does not depend on temperature (in some cases, within a limited temperature range). The term *B* (the mixing term) exists only in a condensed state of the material, in which the atomic states are split by the ligand field [19].

The trigonal crystal field splits states with an even total momentum into states with a less than threefold degeneracy. These states do not have a magnetic moment and, hence, are not split by a magnetic field (for doubly degenerate states, this is valid in the first approximation). Accordingly, there should be neither a diamagnetic term nor a paramagnetic term *C* of the magnetic circular dichroism for either any of the transition splitting components in the trigonal crystal field or for the sum over the whole $J_1 \longrightarrow J_2$ band. However, if the splitting of states in the trigonal crystal field is small, the components of this splitting exhibit a strong *B*-type paramagnetic effect equal in magnitude but opposite in sign with a magneto-optical activity of the order of $\mu_B H/\Delta$, where Δ is the splitting in the crystal field ($\mu_B H \ll \Delta$). The point of inflection on the magnetic circular dichroism curve in the region where the magnetic circular dichroism reverses sign coincides with the position of line A_4 in band *A* and with the position of line B_8 in band *B* (see Figs. 3 and 4, respectively). Hence, it is the splitting of these transitions in the trig-

onal crystal field that accounts for the large alternating magnetic circular dichroism. If these effects originate from the splitting of the excited state, the band-integrated effect should be zero. Otherwise, the integrated effect may be different from zero because of the difference in the population of the splitting components of the ground state in the trigonal crystal field. As a result of the difference between the thermal populations, the integrated magneto-optical activity of the splitting components is of the order of the product $(\mu_B H/\Delta) \times (\Delta/kT) = \mu_B H/kT$ ($\Delta \ll kT$), exactly what is observed in experiment. Although this effect corresponds in magnitude and temperature dependence to the term C, the above reasoning suggests that it is actually a pseudo C effect, because it originates not from the splitting of the ground state levels by the magnetic field but rather from the polarization of transitions in the magnetic field. Thus, the magnetic circular dichroism in band B is predominantly determined by the contribution from the splitting of the excited state, whereas the magnetic circular dichroism in band A is governed primarily by the contribution from the splitting of the ground state in a trigonal crystal field.

REFERENCES

1. W. A. Dollase and R. J. Reeder, Am. Mineral. **71**, 163 (1986).
2. N. I. Leonyuk, E. V. Koporulina, S. N. Barilo, L. A. Kurnevich, and G. L. Bychkov, J. Cryst. Growth **191**, 135 (1998).
3. O. Aloui-Lebbou, C. Goutaudier, S. Kubota, C. Dujardin, M. Th. Cohen-Adad, C. Pedrini, P. Florian, and D. Massiot, Opt. Mater. **16**, 77 (2001).
4. I. Couwenberg, K. Binnemans, H. de Leebeeck, and C. Gorller-Warland, J. Alloys Compd. **27**, 157 (1998).
5. Yongyuan Xu, Xinghong Gong, Yujin Chen, Miaoliang Huang, Zundu Luo, and Yidong Huang, J. Cryst. Growth **252**, 241 (2003).
6. D. Jaque, M. O. Ramirez, L. E. Bausa, J. Garcý Sole, E. Cavalli, A. Speghini, and M. Bettinelli, Phys. Rev. B: Condens. Matter **68**, 035118 (2003).
7. J. B. Gruber, Phys. Rev. B: Condens. Matter **40**, 9464 (1989).
8. A. Braud, IEEE J. Quantum Electron. **34**, 2246 (1998).
9. C. P. Wyss, J. Lumin. **82**, 137 (1999).
10. S. N. Bagaev, Quantum Electron. **30**, 310 (2000).
11. F. Guell, X. Mateos, J. Gavalda, M. Aguilo, F. Diaz, and J. Massons, J. Lumin. **106**, 109 (2004).
12. G. H. Jia, C. Y. Tu, Z. Y. You, J. F. Li, Z. J. Zhu, and B. C. Wu, Solid State Commun. **134**, 583 (2005).
13. Z. S. Xiao, R. Serna, C. N. Afonso, and I. Vickridge, Appl. Phys. Lett. **87**, 111103 (2005).
14. A. P. Ramirez, A. Hayashi, R. J. Cava, R. Siddharthan, and B. S. Shastry, Nature (London) **399**, 333 (1999).
15. M. C. Pujol, F. Guell, X. Mateos, J. Gavalda, R. Sole, J. Massons, M. Aguilo, F. Dýaz, G. Boulon, and A. Brenier, Phys. Rev. B: Condens. Matter **66**, 144304 (2002).
16. L. N. Bezmaternykh, V. L. Temerov, I. A. Gudim, and N. A. Stolbovaya, Crystallogr. Rep. **50** (Suppl. 1), 97 (2005).
17. I. S. Edelman, A. V. Malakhovskii, A. M. Potseluyko, T. V. Zarubina, and A. V. Zamkov, J. Non-Cryst. Solids **306**, 120 (2002).
18. G. F. Koster, J. O. Dimmock, R. G. Wheeler, and H. Statz, *Properties of the Thirty Two Point Groups* (MIT, Cambridge, MA, 1963).
19. A. V. Malakhovskii, Phys. Status Solidi B **159**, 883 (1990).

Translated by G. Skrebtsov